AIAA JOURNAL
Vol. 44, No. 5, May 2006

Avian Wing Geometry and Kinematics

Tianshu Liu*
Western Michigan University, Kalamazoo, Michigan 49008
and
K. Kuykendoll,† R. Rhew,‡ and S. Jones§
NASA Langley Research Center, Hampton, Virginia 23681

The avian wing geometry of a seagull, merganser, teal, and owl extracted from noncontact surface measurements using a three-dimensional laser scanner is presented. The geometrical quantities, including the camber line and thickness distribution of the airfoil, wing planform, chord distribution, and twist distribution, are given in convenient analytical expressions. The avian wing kinematics is recovered from videos of a level-flying seagull, crane, and goose based on a two-jointed arm model in which three characteristic angles are expressed in the Fourier series as a function of time. Therefore, the flapping avian wing with the correct kinematics can be computationally generated for the aerodynamic study of flapping flight.

Introduction

INSPIRED by bird flight, early aviation researchers have studied avian wings as the basics of developing man-made flight vehicles. This methodology is clearly seen in the work of Lilienthal[1] and Magnan.[2] This may be partially the reason why early aircraft designers such as the Wright brothers tended to use thin airfoils by simply simulating bird wings. However, this situation was dramatically changed because relatively thick airfoils (such as Göttingen and NACA airfoils) designed based on theoretical and experimental methods of aerodynamics achieved much higher lift-to-drag ratio at Reynolds numbers in airplane flight. Thus, the study of avian wings became a marginalized topic that only interested a few avian biologists and zoologists. Nachtigall and Wieser[3] measured the airfoil sections of a pigeon's wing. Oehme and Kitzler[4] measured the planform of 14 avian wings and gave an empirical formula for the avian wing chord distribution. Recently, there is renewed interest in low Reynolds number flight and flapping flight in the aerospace community due to the need of developing micro-air-vehicles (MAVs). Hence, it is worthwhile to revisit the problem of the geometry, kinematics, and aerodynamics of avian wings. The objective of this paper is to measure the surface geometry of several avian wings (seagull, merganser, teal, and owl) using a three-dimensional laser scanning system and extract the wing geometrical properties such as the camber line, thickness distribution, planform, chord distribution, and twist distribution. The avian wing kinematics is recovered from videos of several level-flying birds (seagull, crane, and goose) based on a two-jointed arm model for the quarter-chord line of a wing. These data are useful for further aerodynamic study of low Reynolds number biomimetic wings and flapping wings for MAVs.

Laser Scanner on FARO Arm

We used a FARO arm (FARO Technologies, Inc.) to which NVision's three-dimensional noncontact laser scanner is attached for wing surface measurements. The FARO arm itself is a high-accuracy hand-held mechanical device with an exchangeable probe for position and surface measurements. When a NVision three-dimensional laser scanner (NVsision, Inc.) is attached and aligned to the arm, the noncontact measurement capability to acquire high-density point cloud data of a complex surface becomes available. On the FARO arm, the position of the scanner relative to a given coordinate system is known accurately. The accuracy of surface data is within 0.041 mm, and data can be given in the coordinate system chosen. Operating with ModelMaker software, the system works based on the principle of laser stripe triangulation. A laser diode and stripe generator is used to project a laser line onto an object. The line is viewed at an angle by cameras so that height variations on the object can be seen as changes in the line shape. The resulting image of the stripe is a profile that contains the shape information of the object. The software processes video data to capture surface shape in real time at over 23,000 points per second. The NVision scanner uses digital camera synchronization to ensure precise measurements. It works for a variety of materials and colors including black. ModelMaker, Windows-compatible software, outputs data in a variety of CAD formats. This system can generate millions of surface data points. Figure 1 shows a seagull wing and its surface data cloud obtained using this system. (The presented data density is considerably diluted to visualize some features.) This study uses only a subset of data, that is, wing cross-sectional data at selected spanwise locations.

Data Processing

The upper and lower surfaces of an airfoil are expressed as addition and subtraction of the camber line and thickness distribution, $z_{\text{upper}} = z_{(c)} + z_{(t)}$ and $z_{\text{lower}} = z_{(c)} - z_{(t)}$, respectively. To extract the mean camber line from wing surface measurements, we use the Birnbaum-Glauert camber line (see Ref. 5)

$$\frac{z_{(c)}}{c} = \frac{z_{(c)\max}}{c}\eta(1-\eta)\sum_{n=1}^{3} S_n(2\eta-1)^{n-1} \tag{1}$$

where $\eta = x/c$ is the normalized chordwise coordinate, $z_{(c)\max}$ is the maximum camber coordinate, and c is the local wing chord. The thickness distribution is given by[5]

$$\frac{z_{(t)}}{c} = \frac{z_{(t)\max}}{c}\sum_{n=1}^{4} A_n\left(\eta^{n+1} - \sqrt{\eta}\right) \tag{2}$$

where $z_{(t)\max}$ is the maximum thickness coordinate. (The maximum thickness is $2\,z_{(c)\max}$.) For a given set of measured data of wing contour, a rotation and translation transformation is first applied so

Presented as Paper 2004-2186 at the AIAA 24th Aerodynamic Measurement Technology and Ground Testing Conference, Portland, OR, 28 June–1 July 2004; received 23 February 2005; revision received 31 October 2005; accepted for publication 10 November 2005. This material is declared a work of the U.S. Government and is not subject to copyright protection in the United States. Copies of this paper may be made for personal or internal use, on condition that the copier pay the $10.00 per-copy fee to the Copyright Clearance Center, Inc., 222 Rosewood Drive, Danvers, MA 01923; include the code 0001-1452/06 $10.00 in correspondence with the CCC.

*Associate Professor, Department of Mechanical and Aeronautical Engineering, G-220; tianshu.liu@wmich.edu. Member AIAA.
†Quality Assurance Specialist, Research Hardware Validation and Verification Branch.
‡Engineer, Mail Stop 238, Aeronautics Systems Engineering Branch. Member AIAA.
§Biologist, Mail Stop 238, Aeronautics Systems Engineering Branch.

a) Seagull wing

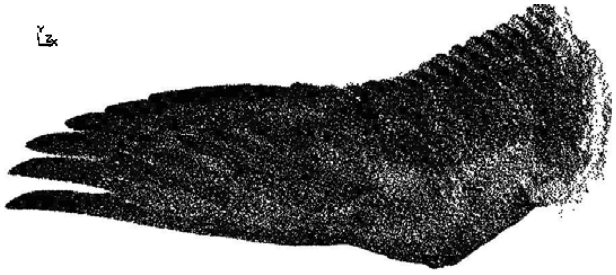

b) Data cloud of the seagull wing surface

Fig. 1 Seagull wing and surface data cloud.

that the geometrical angle of attack becomes zero and the leading edge of the wing section is located at the origin of the local coordinate system. Therefore, the local wing chord, twist angle, $z_{(c)\max}$, $z_{(t)\max}$, and relative position of the leading and trailing edges can be determined. Next, using a least-squares method, we can obtain the coefficients S_n and A_n in Eqs. (1) and (2) for the camber line and thickness distribution. In general, these coefficients are functions of the normalized spanwise coordinate $\xi = 2y/b$, where $b/2$ is the semispan of a wing in a sense of the orthographic projection of the wing. However, when a systematic behavior of the coefficients cannot be found, we use the span-averaged coefficients for the camber line and thickness distribution.

The wing chord distribution can be expressed as

$$c/(b/2) = [c_0/(b/2)][F_{\mathrm{OK}}(\xi) + F_{\mathrm{corr}}(\xi)] \tag{3}$$

where c_0 is the root chord of a wing. The function $F_{\mathrm{OK}}(\xi)$, a correlation given by Oehme and Kitzler[4] for avian wings, is defined as $F_{\mathrm{OK}}(\xi) = 1$ for $\xi \in [0, 0.5]$ and $F_{\mathrm{OK}}(\xi) = 4\xi(1-\xi)$ for $\xi \in [0.5, 1]$. The correction function for a deviation of an individual wing from $F_{\mathrm{OK}}(\xi)$ is

$$F_{\mathrm{corr}}(\xi) = \sum_{n=1}^{5} E_n(\xi^{n+2} - \xi^8)$$

where the coefficients E_n are to be determined. The maximum camber line and thickness coordinates $z_{(c)\max}$ and $z_{(t)\max}$ in Eqs. (1) and (2) can be described by appropriate empirical functions of the spanwise location $\xi = 2y/b$.

The position and kinematics of the quarter-chord line of a wing to a fixed-body coordinate system can be described by a dynamic system $(x_{c/4}, y_{c/4}, z_{c/4}) = (b/2) f_{c/4}(t)$, where t is time. As an approximate model, an avian wing can be described as a multiple-jointed rigid arm system, and its kinematics can be determined.[6,7] In this paper, a simple two-jointed rigid-arm system is adopted to describe the quarter-chord line of an avian wing rather than exactly simulating the more complicated skeleton structure of an avian wing. The use of this two-jointed arm model allows extraction of three characteristic angles determining the kinematics of the quarter-chord line from fronted-viewed videos of level-flying birds. The local twist angle of the airfoil section around the quarter-chord line can be given by $\theta = f_\theta(2x_{c/4}/b, 2y_{c/4}/b, 2z_{c/4}/b)$. Once the geometrical and kinematical parameters in the preceding relations are given, a flapping wing with the correct kinematics can be computationally generated.

Avian Wing Geometry

Seagull

The coefficients S_n and A_n in Eqs. (1) and (2) for the camber line and thickness distribution are extracted using least-squares method from measurements of a seagull wing (Fig. 1). It is found that the coefficients do not show a systematic behavior as a function of the spanwise location, although some variations exist. Thus, we consider the averaged coefficients along the wingspan. Table 1 lists the coefficients S_n and A_n for the seagull wing along with the merganser, teal, and owl wings. Figure 2 shows the normalized camber line and thickness distribution for the seagull wing generated by using the span-averaged coefficients. These distributions exhibit the span-averaged airfoil of the seagull wing over $\xi = 2y/b = 0.166 - 0.772$. For $2y/b > 0.772$, the primaries are separated such that no single, continuous airfoil exists. Figure 3a shows the least-squares estimation residuals in fitting local airfoils $z_{(c)}/c$ and $z_{(t)}/c$ at different spanwise locations. The residuals are 0.002–0.016c. Figure 3b shows the deviations of the span-averaged $z_{(c)}/z_{(c)\max}$ and $z_{(t)}/z_{(t)\max}$ from the local profiles at different spanwise locations in terms of the local maximum values $z_{(c)\max}$ and $z_{(t)\max}$. The deviations are 5–20% of the maximum values. Based on measurements, the maximum camber and thickness coordinates $z_{(c)\max}$ and $z_{(t)\max}$ are decreasing functions of the spanwise location $\xi = 2y/b$, which are empirically expressed as $z_{(c)\max}/c = 0.14/(1 + 1.333\,\xi^{1.4})$ and $z_{(t)\max}/c = 0.1/(1 + 3.546\,\xi^{1.4})$.

The seagull wing planform is shown in Fig. 4. The seagull wing chord distribution, as shown in Fig. 5, is described by Eq. (3), the Oehme and Kitzler's correlation $F_{\mathrm{OK}}(\xi)$ plus a correction function

$$F_{\mathrm{corr}}(\xi) = \sum_{n=1}^{5} E_n(\xi^{n+2} - \xi^8)$$

for local variation, where the coefficients E_n are given in Table 2 for the seagull wing along with the merganser, teal, and owl wings. The ratio between the root chord and semispan for the seagull wing

Table 1 Coefficients for avian airfoil

Coefficient	Seagull	Merganser	Teal	Owl
S_1	3.8735	3.9385	3.9917	3.9733
S_2	−0.807	0.7466	−0.3677	−0.8497
S_3	0.771	1.840	0.0239	−2.723
A_1	−15.246	−23.1743	1.7804	−47.683
A_2	26.482	58.3057	−13.6875	124.5329
A_3	−18.975	−64.3674	18.276	−127.0874
A_4	4.6232	25.7629	−8.279	45.876

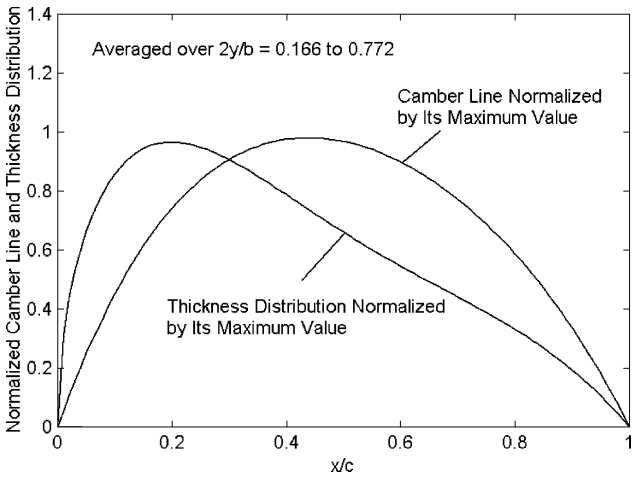

Fig. 2 Camber line and thickness distribution of seagull wing.

Table 2 Coefficients for wing planform

Coefficient	Seagull	Merganser	Teal	Owl
E_1	26.08	39.1	−66.1	6.3421
E_2	−209.92	−323.8	435.6	−7.5178
E_3	637.21	978.7	−1203.0	−70.9649
E_4	−945.68	−1417.0	1664.1	188.0651
E_5	695.03	1001.0	−1130.2	−160.1678

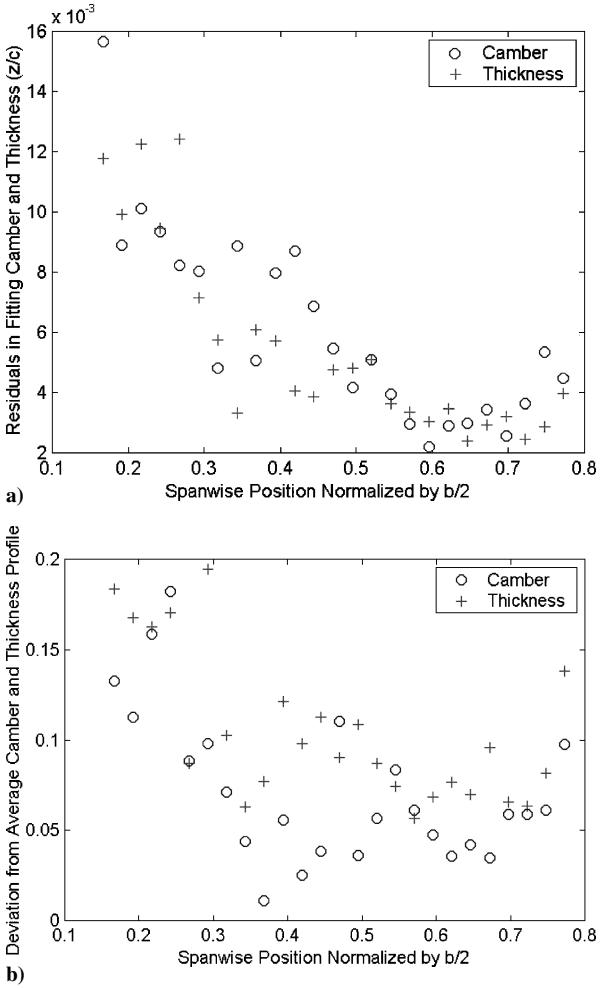

Fig. 3 Fitting errors: a) least-squares residuals in fitting airfoil sections and b) deviation of local profiles from span-averaged profile for seagull wing.

is $c_0/(b/2) = 0.388$. The wing twist relative to the wing root is a function of the spanwise location, which is expressed as an expansion of the Chebyshev polynomials ($T_1 = \xi$, $T_2 = 4\xi^3 - 3\xi$, and $T_3 = 16\xi^5 - 20\xi^3 + 5\xi$), that is,

$$\text{twist(deg)} = \sum_{n=1}^{3} D_n T_n(\xi)$$

where $D_1 = 5.2788$, $D_2 = -4.1069$, and $D_3 = -1.8684$ for the seagull wing. The positive sign of the twist denotes that the wing rotates against the incoming flow. Note that the wing twist presented here is not necessarily intrinsic because not only the twist may be changed in preparing the wing specimen, but also the twist is really a time-dependent variable during flapping. Using the preceding relations obtained from measurements, we are able to generate the seagull wing surface as shown in Fig. 6a, where a two-jointed arm model is used for the quarter-chord line. Even though the real wing has separated primaries near the wing tip, it is assumed that the airfoil section remains the same near the wing tip while the maximum thickness decreases.

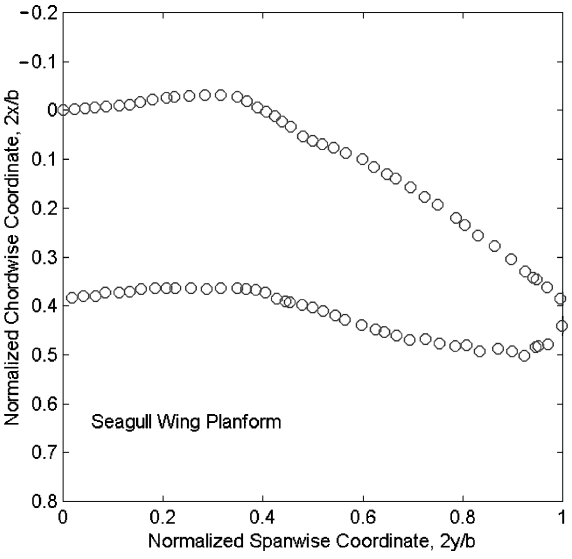

Fig. 4 Seagull wing planform.

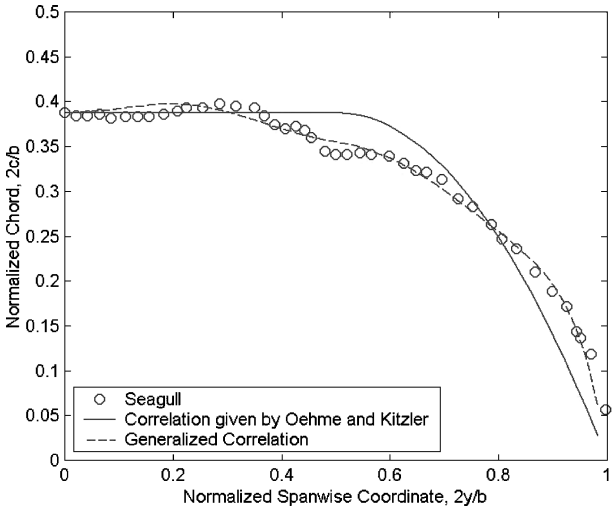

Fig. 5 Chord distribution of seagull wing.

Merganser, Teal, and Owl

Figure 7 shows the normalized camber line and thickness distribution for the merganser wing generated using the averaged coefficients given in Table 1. The wing thickness is very small (considered to be zero) near the trailing edge ($x/c > 0.9$). The least-squares estimation residuals in fitting local airfoils at different spanwise locations are less than $0.01c$. The deviations of the span-averaged $z_{(c)}/z_{(c)\max}$ and $z_{(t)}/z_{(t)\max}$ from the local profiles at different spanwise locations are less than 30%. The maximum camber and thickness coordinates $z_{(c)\max}$ and $z_{(t)\max}$ is given by the empirical expressions $z_{(c)\max}/c = 0.14/(1 + 1.333\ \xi^{1.4})$ and $z_{(t)\max}/c = 0.05/(1 + 4\ \xi^{1.4})$ as a decreasing function of the spanwise location $\xi = 2y/b$. Figures 8 and 9 show the merganser wing planform and the distribution of the wing chord, respectively. The ratio between the root chord and semispan for the merganser wing is $c_0/(b/2) = 0.423$. The wing twist as a function of the spanwise location is expressed as an expansion of the Chebyshev polynomials ($T_1 = \xi$, $T_2 = 4\xi^3 - 3\xi$, and $T_3 = 16\xi^5 - 20\xi^3 + 5\xi$), that is,

$$\text{twist(deg)} = \sum_{n=1}^{3} D_n T_n(\xi)$$

where $D_1 = 30.9953$, $D_2 = -3.2438$, and $D_3 = -0.2076$. The generated merganser wing surface is shown in Fig. 6b.

Figure 10 shows the normalized camber line and thickness distribution for the teal wing generated using the averaged coefficients given in Table 1. The least-squares estimation residual in fitting

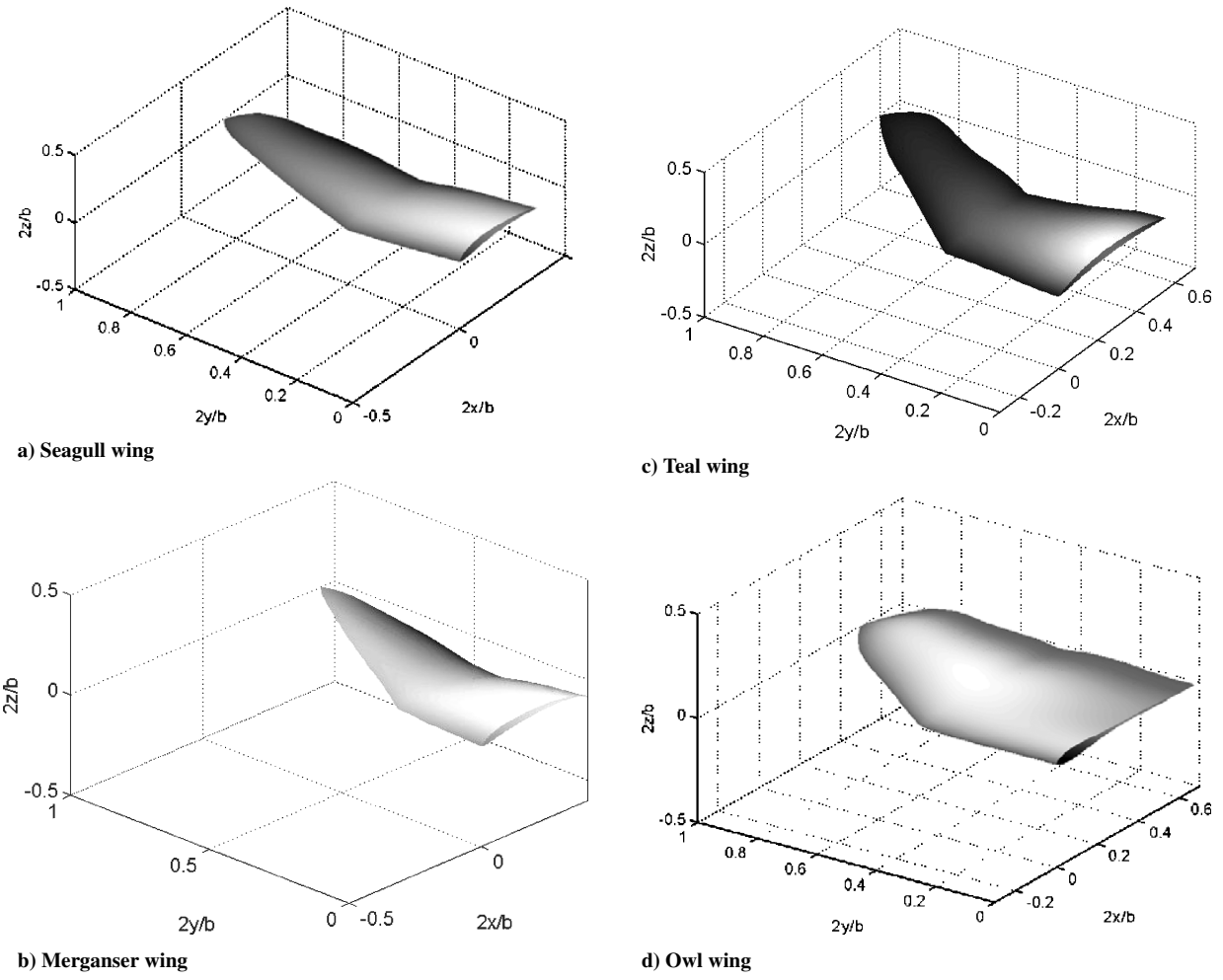

Fig. 6 Generated avian wing surfaces.

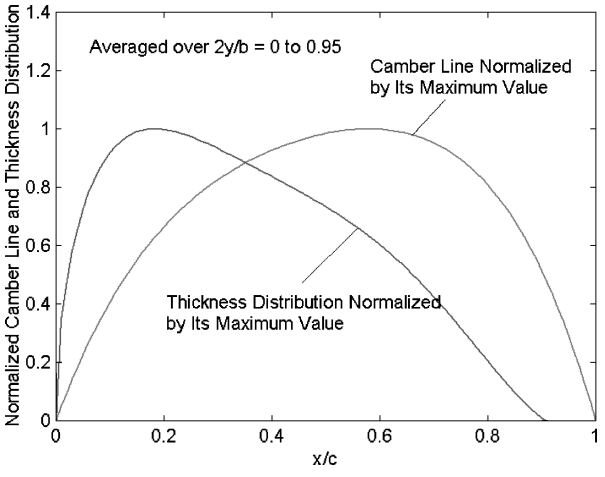

Fig. 7 Camber line and thickness distribution of merganser wing.

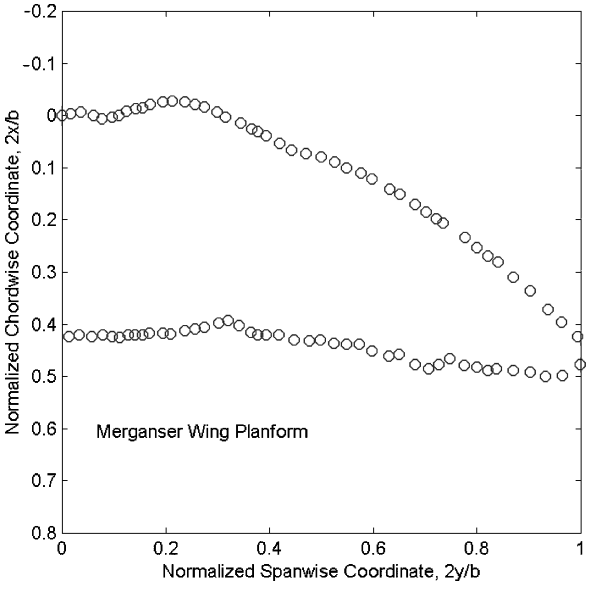

Fig. 8 Merganser wing planform.

local airfoils is less than $0.01c$. The deviations of the span-averaged $z_{(c)}/z_{(c)\max}$ and $z_{(t)}/z_{(t)\max}$ from the local profiles are less than 20%. The maximum camber and thickness coordinates $z_{(c)\max}$ and $z_{(t)\max}$ are given by the empirical expressions $z_{(c)\max}/c = 0.11/(1+4\,\xi^{1.4})$ and $z_{(t)\max}/c = 0.05/(1+4\,\xi^{1.4})$ as a decreasing function of the spanwise location $\xi = 2y/b$. Figures 11 and 12 show, respectively, the teal wing planform and the measured distribution of the wing chord along with the fitted results by Eq. (3) where the coefficients E_n in $F_{\text{corr}}(\xi)$ are given in Table 2. The ratio between the root chord and semispan is $c_0/(b/2) = 0.545$. The wing twist is less than 2 deg along the span. The teal wing surface generated using the preceding relations is shown Fig. 6c.

Figure 13 shows the normalized camber line and thickness distribution for the owl wing generated using the averaged coefficients given in Table 1. The least-squares estimation residual in fitting local airfoils is less than $0.01c$. The deviations of the span-averaged $z_{(c)}/z_{(c)\max}$ and $z_{(t)}/z_{(t)\max}$ from the local profiles are less than 20%. Interestingly, the owl wing is very thin over a large portion of the wing ($x/c = 0.3 - 1.0$) and it is basically a single layer of the primary feathers; the thickness distribution is mainly concentrated in

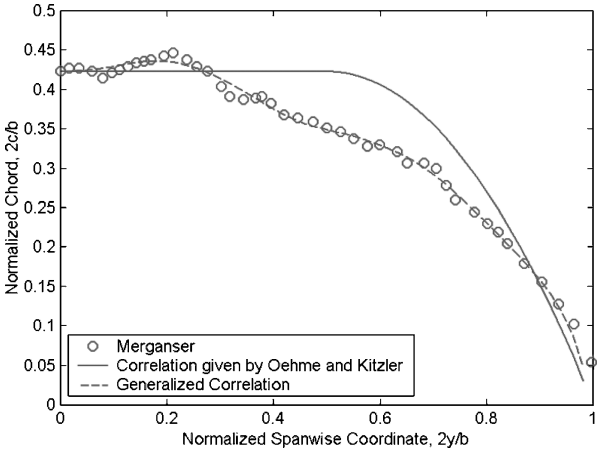

Fig. 9 Chord distribution of merganser wing.

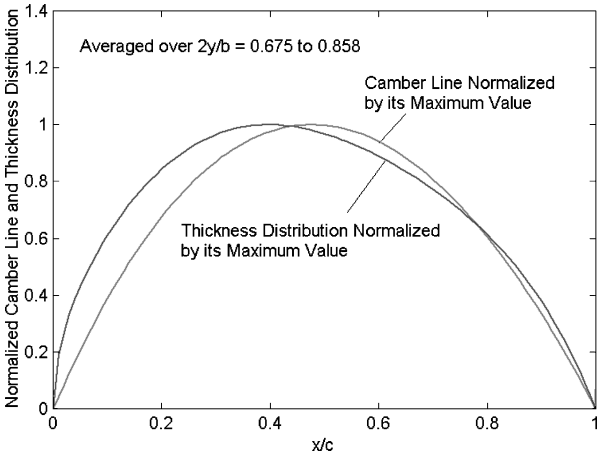

Fig. 10 Camber line and thickness distribution of teal wing.

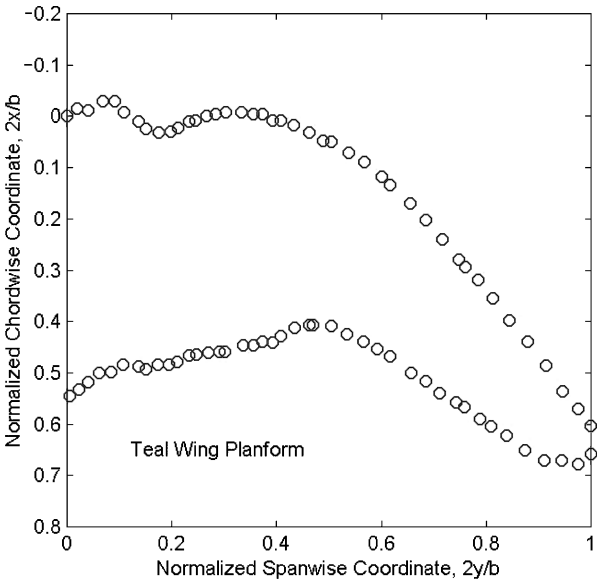

Fig. 11 Teal wing planform.

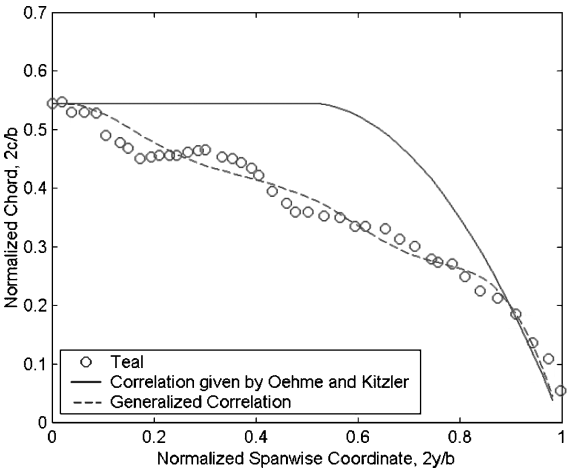

Fig. 12 Chord distribution of teal wing.

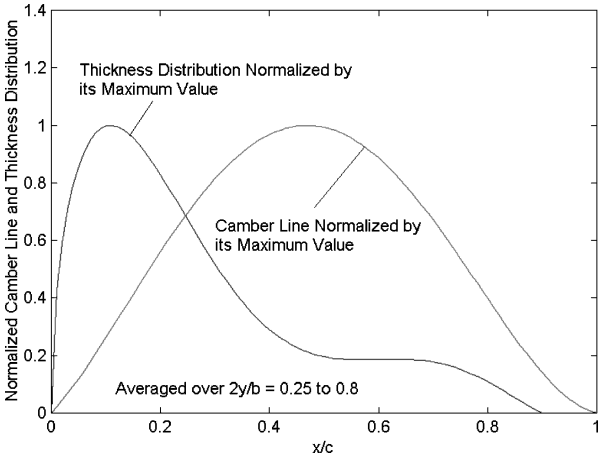

Fig. 13 Camber line and thickness distribution of owl wing.

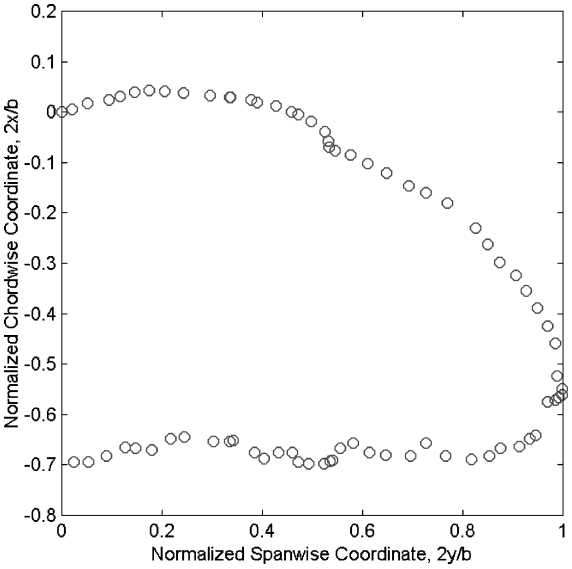

Fig. 14 Planform of owl wing.

the front portion of the airfoil. The wing thickness is considered to be zero near the trailing edge ($x/c > 0.9$). The maximum camber and thickness coordinates $z_{(c)\max}$ and $z_{(t)\max}$ are given by the empirical expressions $z_{(c)\max}/c = 0.04[1 + \tanh(1.8\xi - 0.5)]$ and $z_{(t)\max}/c = 0.04/(1 + 1.78\ \xi^{1.4})$ as a function of the spanwise location $\xi = 2y/b$. In contrast to other wings, the maximum chamber coordinate for the owl wing increases along the span, at least for this wing specimen. Figures 14 and 15 show the owl wing planform and the measured wing chord distribution along with the fitted results by Eq. (3), where the coefficients E_n in $F_{\text{corr}}(\xi)$ are given in Table 2. The ratio between the root chord and semispan for the owl wing is $c_0/(b/2) = 0.677$, indicating a small wing aspect ratio. The wing twist is less than 2 deg along the span. The owl wing surface generated using the preceding relations is shown in Fig. 6d. It remains to be seen whether the unique structure of the owl wing is related to the owl's silent flight.[8]

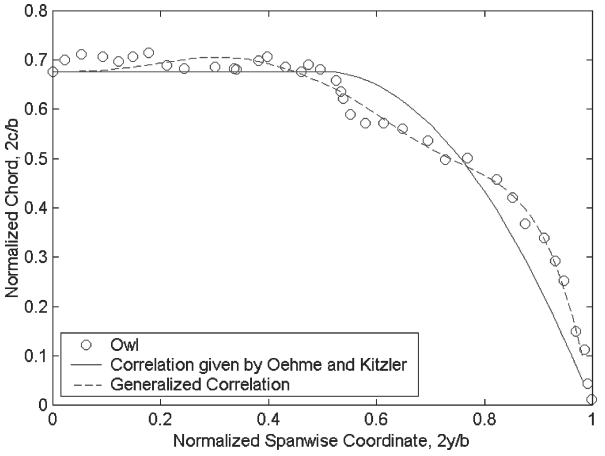

Fig. 15 Chord distribution of owl wing.

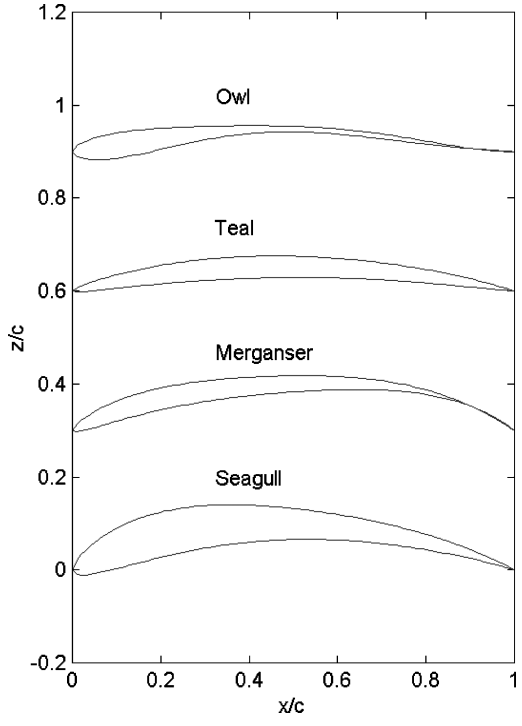

Fig. 16 Airfoil sections of avian wings at $2y/b = 0.4$.

Comparison with Low-Reynolds-Number Airfoil

Figure 16 shows the typical seagull, merganser, teal, and owl wing sections at $2y/b = 0.4$ that are highly cambered. The seagull and merganser airfoils are similar to the high-lift, low-Reynolds-number airfoil S1223 described by Selig et al.[9] Figure 17 shows a comparison of the S1223 airfoil with the seagull and merganser airfoils with the same maximum camber line and thickness coordinates ($z_{(c)\max}/c = 0.0852$ and $z_{(t)\max}/c = 0.0579$). Interestingly, the averaged airfoil of the seagull and merganser airfoils is even more similar to the S1223 airfoil. Figure 18 shows a comparison of the pressure coefficient distributions between the S1223, seagull, and merganser airfoils given by the XFOIL code.[10] These pressure distributions are similar, but the S1223 airfoil has lower pressures on the upper surface near $x/c = 0.2$ and the trailing edge.

Avian Wing Kinematics

Front-Projected Quarter-Chord Line

For simplicity, the kinematics of a flapping wing is considered as a superposition of the motion of the quarter-chord line of the wing and relative rotation of local airfoil sections around the quarter-chord line. From videos of a level-flying bird taken by a camera viewing the bird front directly, we are able to recover approximately

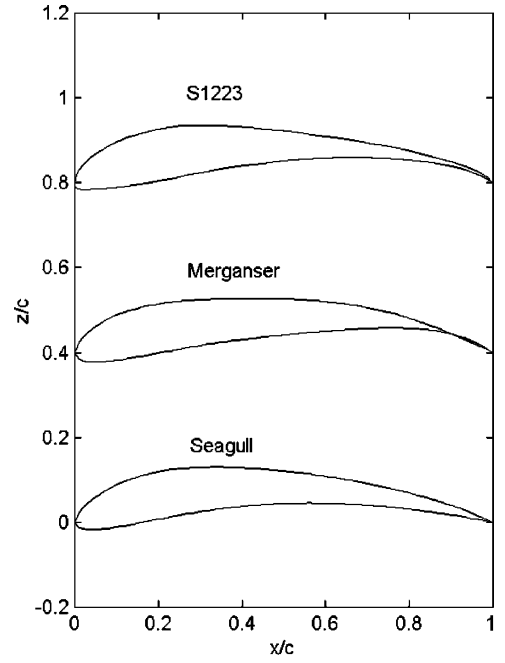

Fig. 17 High-lift, low-Reynolds airfoil S1223 compared to the seagull and merganser airfoils with same maximum camber line and thickness coordinates.

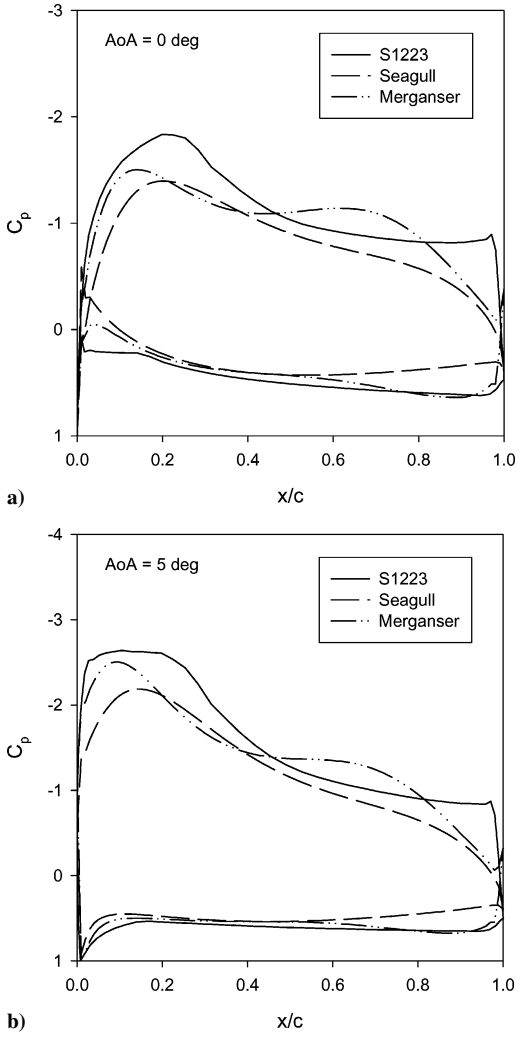

Fig. 18 Pressure coefficient distributions for seagull and merganser airfoils along with that for S1223 at angle of attack a) 0 and b) 5 deg.

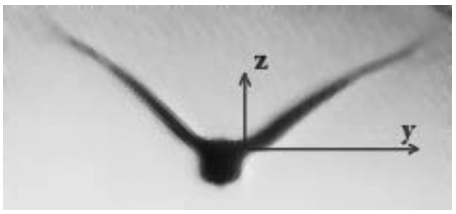

Fig. 19 Level-flying bird (crane) viewed by camera directly from front.

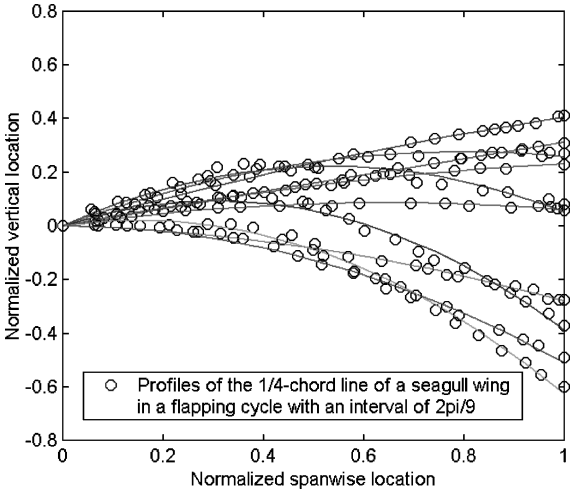

Fig. 20 Profiles of front-projected quarter-chord line of flapping seagull wing at different instants.

a time sequence of the front-projected profiles of the quarter-chord line of the flapping wing. Figure 19 shows a typical image of a level-flying bird (crane) viewed directly from the front and a local coordinate system used to describe the profiles. A front-projected wing in images is a line with a finite thickness that is approximately considered as the front-projected quarter-chord line. The profile of the front-projected quarter-chord line of a flapping wing can be reasonably described by a second-order polynomial:

$$z_{\frac{1}{4}}/(b/2) = A_1(\omega t)[y_{\frac{1}{4}}/(b/2)] + A_2(\omega t)[y_{\frac{1}{4}}/(b/2)]^2 \quad (4)$$

where the coefficients and the semispan are given by the Fourier series as a function of the nondimensional time ωt (where ω is the circular frequency of flapping),

$$A_1(\omega t) = C_{10} + \sum_{n=1}^{2}[C_{1n}\sin(n\omega t) + B_{1n}\cos(n\omega t)]$$

$$A_2(\omega t) = C_{20} + \sum_{n=1}^{2}[C_{2n}\sin(n\omega t) + B_{2n}\cos(n\omega t)]$$

$$\frac{b(\omega t)/2}{\max(b/2)} = C_{b0} + \sum_{n=1}^{2}[C_{bn}\sin(n\omega t) + B_{bn}\cos(n\omega t)] \quad (5)$$

Here, $b/2$ is defined as the semispan of an orthographically projected flapping wing on the horizontal plane. Therefore, $b/2$ is a time-dependent function in a flapping cycle. The maximum value of $b/2$ is achieved roughly at the moment when a flapping wing is parallel to the horizontal plane. We assume that $\omega t = 0$ corresponds to the position of a wing at the beginning of the downstroke (or the end of the upstroke). Figure 19 shows the wing position at $\omega t = 0$.

A time sequence of images of a flying seagull taken by a camera directly from the bird front (acquired from Oceanfootage.com) is processed; the profiles of the front-projected wing (or quarter-chord line) are obtained by manually tracing the wing in digitized images. Equation (4) is used to fit data of the successive profiles, and the coefficients in Eq. (5) are determined. Figure 20 shows the measured profiles of the front-projected quarter-chord line of a flapping seagull wing and the corresponding polynomial fits at 10 instants (an interval of $2\pi/9$) in a flapping cycle $\omega t \in [0, 2\pi]$. The profiles can be reasonably described by a second-order polynomial Eq. (4) with the time-dependent coefficients. Figures 21 and 22 show the recovered coefficients in Eq. (5) and the orthographically projected semispan $b/2$ that are fitted by the Fourier series, respectively. The coefficients in Eq. (5) extracted from measurements are listed in Table 3 for a flapping seagull wing along with the crane and goose wings.

Table 3 Coefficients for front-projected quarter-chord line

Coefficient	Seagull	Crane	Goose
C_{10}	0.3756	0.3639	0.4511
C_{11}	−0.3242	−0.2938	−0.2819
B_{11}	0.1920	0.4050	0.3008
C_{12}	0.0412	−0.0465	0.0254
B_{12}	−0.1095	−0.0331	−0.0835
C_{20}	−0.4674	−0.4294	−0.4605
C_{21}	0.3631	0.4469	0.4516
B_{21}	0.2884	0.1442	0.1912
C_{22}	−0.0661	0.0135	−0.0845
B_{22}	0.0553	0.0691	0.1154
C_{b0}	0.7978	0.8390	0.8999
C_{b1}	0.1751	0.0885	0.0666
B_{b1}	0.0461	0.0301	0.0126
C_{b2}	0.0042	−0.0888	−0.0505
B_{b2}	−0.0218	−0.0407	−0.0095
C_{L0}	0.8718	0.9310	0.9948
C_{L1}	0.1420	0.0359	0.0013
B_{L1}	−0.0111	0.0111	−0.0013
C_{L2}	0.0190	−0.0675	−0.0083
B_{L2}	0.0113	−0.0093	0.0122

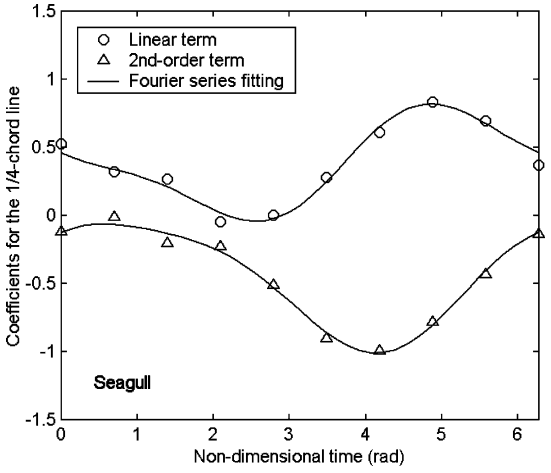

Fig. 21 Polynomial coefficients of front-projected quarter-chord line of flapping seagull wing as function of time.

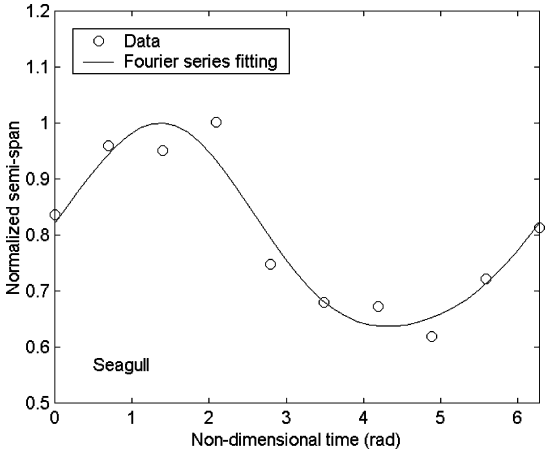

Fig. 22 Orthographically projected semispan $b/2$ normalized by max($b/2$) for flapping seagull wing as function of time.

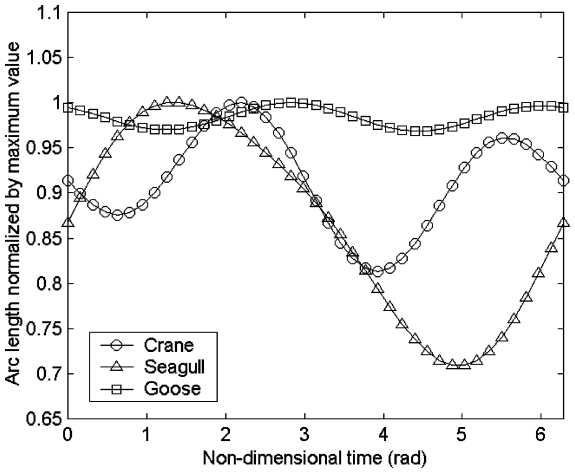

Fig. 23 Normalized arc length of front-projected quarter-chord line of flapping seagull, crane, and goose wings as function of time.

As shown in Fig. 22, the orthographically projected semispan $b/2$ on the horizontal plane varies with time. At $\omega t = 0$, the position of the wing is at the beginning of the downstroke. The wing is approximately parallel to the horizontal plane at $\omega t \approx 1.5$ and $b/2$ reaches the maximal value. The minimal value of $b/2$ is at $\omega t \approx 4.3$. The downstroke spans about 68% of a flapping cycle, whereas the upstroke takes 32% of a cycle. The variation of $b/2$ with time depends on not only the orthographical projection, but also a change of the wing planform due to wing flexion during flapping. We calculate the arc length of the front-projected quarter-chord line as a function of time using Eqs. (4) and (5). In fact, a change in the arc length of the front-projected quarter-chord line represents a change of the wing planform due to wing flexion. Figure 23 shows the arc length of the projected quarter-chord line as a function of time for the flapping seagull, crane, and goose wings. For a seagull, its wing is most extended at $\omega t \approx 1.2$, whereas it is most folded at $\omega t \approx 5$. The normalized arc length of the front-projected quarter-chord line is described by the Fourier series

$$\frac{L_{\text{proj}}(\omega t)}{\max(L_{\text{proj}})} = C_{L0} + \sum_{n=1}^{2}[C_{Ln}\sin(n\omega t) + B_{Ln}\cos(n\omega t)] \quad (6)$$

For the flapping seagull wing, the coefficients in Eq. (6) are also listed in Table 3. These results will be used to reconstruct the wing kinematics based on a two-jointed arm model.

A time sequence of images of a level-flying crane and a flying bar-headed goose taken by a camera directly from the bird front are obtained by digitizing a clip of the video "The Life of Birds" produced by the BBC and the documentary "Winged Migration," respectively. The images from these nonscientific videos are used because high-speed images of large birds flying in a controllable environment such as a wind tunnel are not available. Thus, it is assumed that the birds observed in the nature were in cruising flight in which the cruising speed can be estimated based on the scaling laws in terms of the weight. The profiles of the front-projected quarter-chord line are recovered. The coefficients in Eqs. (5) and (6) for a flapping crane wing and a goose wing are listed in Table 3. The normalized arc lengths of the front-projected quarter-chord line of the flapping crane and goose wings are shown in Fig. 23. As shown in Fig. 23, the normalized arc length of the front-projected quarter-chord line of the flapping goose wing does not vary much compared with the flapping seagull and crane wings. This means that, relatively, the goose wing does not flex much during flapping in level flight.

Two-Jointed Arm Model

In general, the skeleton structure is described as a three-jointed arm system. However, for level flapping flight, the wing kinematics can be simplified. In this case, to describe the quarter-chord line of a flapping wing, we use a two-jointed arm model that consists of two rigid-jointed rods. As shown in Fig. 24, rod 1 rotates around the point O_1 in a body coordinate system where the origin O_1 is located at the wing root, and the plane YO_1Z is defined as the rotational plane of rod 1. Thus, the motion of rod 1 has only one degree of freedom and the position of rod 1 is given by the flapping angle ψ_1. In contrast, the motion of rod 2 has two degrees of freedom and is given by the angles ψ_2 and ϕ_2. In Fig. 24, the line O_2T' is the orthographic projection of rod 2 (or the line O_2T) on the plane YO_1Z. The angle ψ_2 is the angle between rod 1 and the line O_2T' on the plane YO_1Z, which basically determines the flapping magnitude of rod 2 relative to rod 1. The angle ϕ_2 is the angle between rod 2 and the line O_2T', which describes the flexion of a wing (the outer portion of a wing). Figure 25 shows the projected views of a two-jointed arm system. In Fig. 25c, the angle $\phi_{2\perp} = \phi_2/\cos(\psi_1 - \psi_2)$ is the orthographic projection of the angle ϕ_2 on the horizontal plane XO_1Y. This simple two-jointed arm model allows the recovery of the three-dimensional kinematics of a flapping wing from measurements of the front-projected quarter-chord line. In addition, it can serve as a straightforward model for designing and analyzing a mechanical flapping wing.

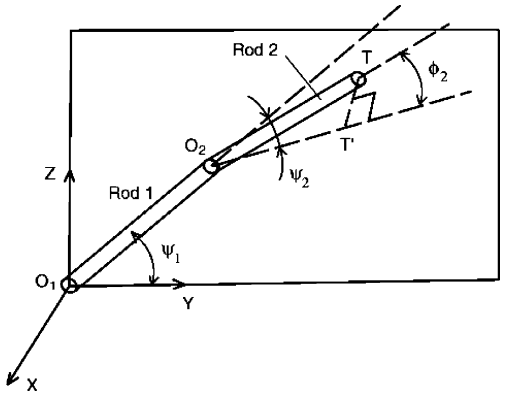

Fig. 24 Two-jointed arm system.

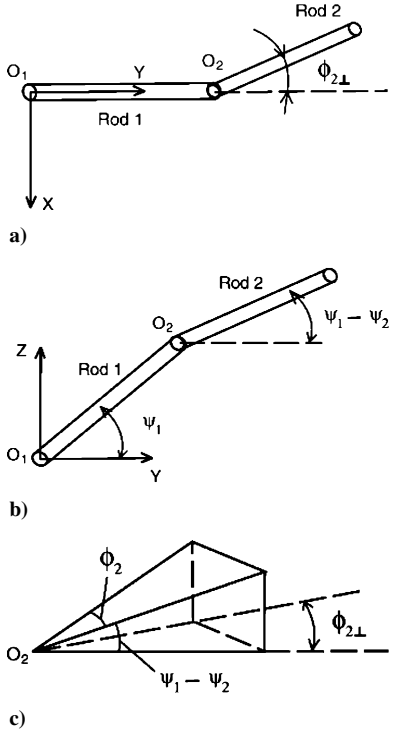

Fig. 25 Projected views of two-jointed arm system: a) top view, b) side view, and c) meaning of angle $\phi_{2\perp}$.

The coordinates of the end point O_2 of rod 1 are

$$X_{O_2} = 0, \qquad Y_{O_2} = L_1\cos(\psi_1), \qquad Z_{O_2} = L_1\sin(\psi_1) \quad (7)$$

where L_1 is the length of rod 1. The position of rod 1 is described by

$$X = 0, \qquad Z = Y \tan(\psi_1) \tag{8}$$

where $Y \in [0, L_1 \cos(\psi_1)]$. The position of rod 2 is given by

$$X = -\left(Y - Y_{O_2}\right) \tan[\phi_2/\cos(\psi_1 - \psi_2)]$$

$$Z = Z_{O_2} + \left(Y - Y_{O_2}\right) \tan(\psi_1 - \psi_2) \tag{9}$$

where $Y \in [L_1 \cos(\psi_1), b/2]$. Note that $b/2$ is the orthographically projected semispan on the horizontal plane XO_1Y. Therefore, we know that the projected semispan is $b/2 = L_1 \cos(\psi_1) + L_2 \cos(\phi_2) \cos(\psi_1 - \psi_2)$. In a two-jointed arm system, the normalized arc length of the front-projected quarter-chord line is

$$L_{\text{proj}}(\omega t)/\max(L_{\text{proj}}) = r_1 + r_2 \cos(\phi_2) \tag{10}$$

where $r_1 = L_1/\max(L_{\text{proj}})$ and $r_2 = L_2/\max(L_{\text{proj}})$ are the relative lengths of rods 1 and 2. Clearly, for the fixed values of r_1 and r_2, the arc length of the front-projected quarter-chord line is solely related to the angle ϕ_2. The kinematics of a two-jointed arm system is determined by three characteristic angles ψ_1, ψ_2, and ϕ_2.

Recovery of Characteristic Angles ψ_1, ψ_2, and ϕ_2

A two-jointed arm model uses two pieces of straight line to approximate the profile of the quarter-chord line of a wing. Because the flapping angles ψ_1 and ψ_2 are on the plane YO_1Z, they can be estimated directly from the measured profile of the front-projected quarter-chord line when $r_1 = L_1/\max(L_{\text{proj}})$ and $r_2 = L_2/\max(L_{\text{proj}})$ are given. The angle ϕ_2 can be extracted from the measured arc length of the front-projected quarter-chord line using Eqs. (6) and (10). Figure 26 shows the recovered angles ψ_1, ψ_2, and ϕ_2, as a function of time for the flapping seagull wing. The characteristic angles ψ_1, ψ_2, and ϕ_2 for the following coefficients are expressed as the Fourier series:

$$\psi_1(\omega t) = C_{\psi 10} + \sum_{n=1}^{2} [C_{\psi 1n} \sin(n\omega t) + B_{\psi 1n} \cos(n\omega t)]$$

$$\psi_2(\omega t) = C_{\psi 20} + \sum_{n=1}^{2} [C_{\psi 2n} \sin(n\omega t) + B_{\psi 2n} \cos(n\omega t)]$$

$$\phi_2(\omega t) = C_{\phi 20} + \sum_{n=1}^{2} [C_{\phi 2n} \sin(n\omega t) + B_{\phi 2n} \cos(n\omega t)] \tag{11}$$

The estimated coefficients in Eq. (11) are given in Table 4 for the flapping seagull, crane, and goose wings. Here, we assume that

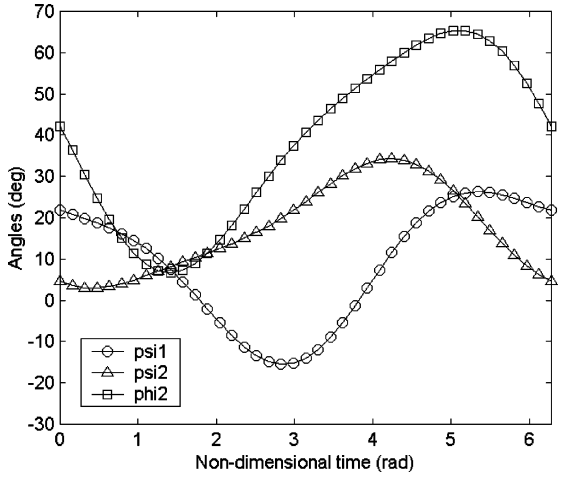

Fig. 26 Characteristic angles ψ_1, ψ_2, and ϕ_2 as function of time for seagull wing kinematics.

Table 4 Coefficients for characteristic angles of wing kinematics

Coefficient	Seagull	Crane	Goose
$C_{\psi 10}$	8.4654	8.3065	12.2528
$C_{\psi 11}$	−8.5368	−4.4519	−3.7150
$B_{\psi 11}$	17.8798	25.3910	21.1873
$C_{\psi 12}$	1.0898	−1.8092	−0.6432
$B_{\psi 12}$	−4.5880	−0.5889	−2.3054
$C_{\psi 20}$	17.3083	17.0661	20.0863
$C_{\psi 21}$	−11.0122	−17.3404	−18.6807
$B_{\psi 21}$	−9.6131	−4.0066	−7.3848
$C_{\psi 22}$	1.3128	−3.7029	1.3467
$B_{\psi 22}$	−3.0183	−4.5122	−6.1507
$C_{\phi 20}$	38.4179	32.2311	13.5235
$C_{\phi 21}$	−28.0553	−8.6004	−0.7494
$B_{\phi 21}$	0.7664	−0.34280	1.2524
$C_{\phi 22}$	−4.1032	15.2213	4.3138
$B_{\phi 22}$	3.0125	2.6910	−6.3023

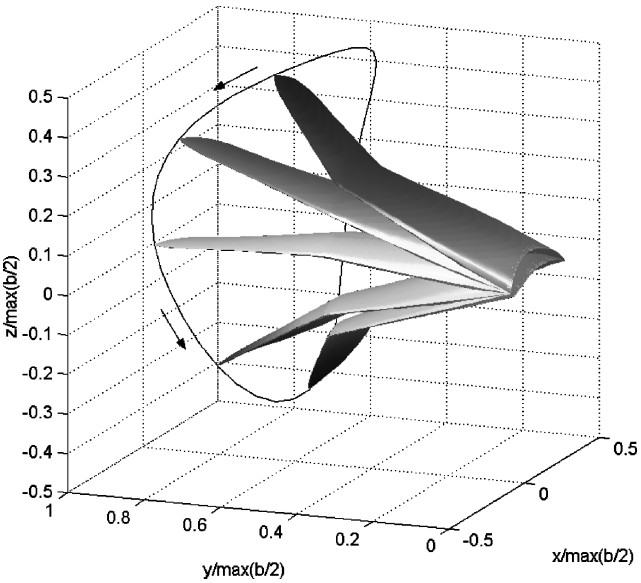

Fig. 27 Reconstructed flapping seagull wing at $\omega t = 0$, $\pi/4$, $\pi/2$, $3\pi/4$, and π.

$r_1 = 0.5$ and $r_2 = 0.5$. The units of the angles ψ_1, ψ_2, and ϕ_2 in Eq. (11) are in degrees.

Reconstruction of a Flapping Wing

Once the wing geometry (airfoil sections, planform, chord distribution, and twist distribution) and the kinematics of the quarter-chord line of a wing are given, a flapping wing can be reconstructed in the three-dimensional object space by superimposing the airfoil sections on the moving quarter-chord line. Note that the wing twist distribution in flapping is not recovered in this work. Measurements of the dynamic wing twist distribution require considerable videogrammetric processing on a time sequence of images taken from two cameras simultaneously viewing a flapping wing of a level-flight bird on which a sufficient number of suitably distributed targets are attached. Such measurements are difficult for flying birds in an uncontrollable environment. In computational simulations, however, the wing twist can be treated as a variable to achieve the maximum aerodynamic efficiency. Here, it is simply assumed that the wing twist is fixed during flapping. Using Eqs. (1–3), (8), (9), and (11) with the recovered coefficients for a seagull wing, we reconstruct a flapping seagull wing that is shown at several instants in Fig. 27. The trajectory of the moving tip of the seagull wing is also shown in Fig. 27.

Conclusions

The surface geometry of the seagull, merganser, teal, and owl wings are measured by using a three-dimensional laser scanner.

From measurements, the airfoil camber line, airfoil thickness distribution, wing planform, and twist distribution are extracted. The accuracy of metric measurements using the laser scanner is about 0.041 mm. The residual of least-squares estimation in fitting airfoil sections is about 2×10^{-3}–20×10^{-3} in terms of the local chord. Because the estimated coefficients for the camber line and thickness distribution do not exhibit a systematic behavior along the wingspan, the averaged values of these coefficients along the wingspan are given, which define the averaged airfoil for an avian wing. The deviation of the local airfoil camber line and thickness distribution from the span-averaged ones is about 5–20% of their maximum values. The seagull and merganser airfoils are similar to a high-lift, low-Reynolds-number airfoil. The teal airfoil has a relatively symmetric thickness distribution around the midchord. The owl airfoil is very thin over 0.3–1.0 chord, and the thickness distribution is mainly concentrated in the front portion of the airfoil.

The kinematics of a flapping wing is considered as a superposition of the motion of the quarter-chord line of the wing and relative rotation of local airfoil sections around the quarter-chord line. The profiles of the front-projected quarter-chord line at different instants are measured from videos of a level-flying bird. Then, based on a two-jointed arm model, the kinematics of the quarter-chord line in the three-dimensional object space is recovered and described in convenient analytical expressions for the flapping seagull, crane, and goose wings. The wing geometry and kinematics given in this paper can be used for the preliminary design of flapping MAVs, and they provide a foundation for further experimental and computational studies to understand the aerodynamic aspects of flapping flight.

Acknowledgment

We thank Harold Cones of Christopher Newport University for providing the seagull, merganser, teal, and owl wings.

References

[1]Lilienthal, O., *Birdflight as the Basis of Aviation*, Markowski International, Hummestown, PA, 2001.

[2]Magnan, A., Bird Flight and Airplane Flight, NASA TM-75777, 1980.

[3]Nachtigall, W., and Wieser, J., "Profilmessungen am Taubenflügel," *Zeitschrift für vergleichende Physiologies*, Vol. 52, 1966, pp. 333–346.

[4]Oehme, H., and Kitzler, U., "On the Geometry of the Avian Wing," *Studies on the Biophysics and Physiology of Avian Flight II*, NASA TT-F-16901, Feb. 1975.

[5]Riegels, F. W., *Aerofoil Sections*, Butterworths, London, 1961, Chaps. 1, 7.

[6]Asada, H., and Slotine, J.-J. E., *Robot Analysis and Control*, Wiley, New York, 1986, Chaps. 2, 3.

[7]Zinkovsky, A. V., Shaluha, V. A., and Ivanov, A. A., *Mathematical Modeling and Computer Simulation of Biomechanical Systems*, World Scientific, Singapore, 1996, Chaps. 1, 2.

[8]Lilley, G. M., "A Study of the Silent Flight of the Owl," AIAA Paper 98-2340, June 1998.

[9]Selig, M. S., Guglielmo, J. J., Broeren, A. P., and Giguere, P., *Summary of Low-Speed Airfoil Data*, Vol. 1, SoarTech, Virginia Beach, VA, 1995, Chap. 4.

[10]Drela, M., "XFOIL: An Analysis of and Design System for Low Reynolds Number Airfoils," *Conference on Low Reynolds Number Airfoil Aerodynamics*, Notre Dame, IN, 1989, pp. 1–12.

C. Kaplan
Associate Editor